Fluid dynamics of the larval zebrafish pectoral fin and the role of fin bending in fluid transport

2013 Bioinspir. Biomim. 8 016002

(http://iopscience.iop.org/1748-3190/8/1/016002)

Bioinspir. Biomim. **8** (2013) 016002 (11pp) doi:10.1088/1748-3182/8/1/016002

Fluid dynamics of the larval zebrafish pectoral fin and the role of fin bending in fluid transport

Matthew H Green[1], **Oscar M Curet**[2,3], **Neelesh A Patankar**[2] **and Melina E Hale**[1,4]

[1] Committee on Computational Neuroscience, University of Chicago, Chicago, IL 60637, USA
[2] Department of Mechanical Engineering, Northwestern University, Evanston, IL 60208, USA
[3] Ocean and Mechanical Engineering, Florida Atlantic University, Boca Raton, FL 33431, USA
[4] Department of Organismal Biology and Anatomy, University of Chicago, Chicago, IL 60637, USA

E-mail: m.hobson.green@gmail.com

Received 5 June 2012
Accepted for publication 15 November 2012
Published 5 December 2012
Online at stacks.iop.org/BB/8/016002

Abstract
Larval zebrafish beat their pectoral fins during many behaviors including low-speed swimming and prey tracking; however, little is known about the functions of these fin movements. Previously, we found experimental support for the function of larval fins in mixing of fluid near the body, which may enhance respiration by diffusion of dissolved oxygen across the skin. Here we use computational fluid dynamics to analyze fluid flow due to the pectoral fin movement. The pectoral fins bend along their proximodistal axis during abduction (fin extension), but remain nearly rigid during adduction (fin flexion). We hypothesize that this asymmetry in bending is critical for fluid mixing near the body and test the effects of fin bending with our simulations. For normal fin beats, we observed similar flow patterns in simulations and experiments. Flow patterns showed fluid stretching and folding, indicative of mixing. When proximodistal bending was removed from fin motion, fins were less effective at transporting fluid in a posterior direction near the body surface, but lateral mixing of fluid near the body was unaffected. Our results suggest that fin bending enhances posterior transport of fluid along the body surface, which may act to aid respiration in combination with lateral stretching and folding of fluid.

S Online supplementary data available from stacks.iop.org/BB/8/016002/mmedia

1. Introduction

Viscosity-dominated low Reynolds number environments present significant challenges to fluid transport and mixing for the biological and engineered systems that must function in them (e.g. mixing in microfluidic channels (Strook *et al* 2002)). Life in low and intermediate Reynolds numbers is common for the small post-hatching larvae of many fish species (e.g. Vlyman 1974, Weihs 1980, Hale 1996, Müller and Videler 1996, McHenry and Lauder 2006). An experimental, flow visualization study of rhythmic axial swimming in larval zebrafish has demonstrated a substantial boundary layer enveloping the animal that is comparable in size to the animal's body width (Müller *et al* 2008). These conditions near the surface of the body have significant consequences for respiration. Many larval fish, including zebrafish, respire cutaneously, relying on diffusion at the skin–water interface to supply the body with oxygen (e.g. Hunter 1972, Weihs 1980, Liem 1981). Limited fluid mixing at the body surface, due to the presence of a boundary layer that engulfs the body, would limit dissolved oxygen exchange at the skin. Here we examine mechanisms for low Reynolds number fluid mixing in larval zebrafish, a model species in studies of motor control and movement.

Experimental and theoretical investigations have suggested that under hypoxic conditions, oxygen supply can be rapidly increased by mixing of new, oxygen-rich fluid into the region surrounding the surface of the body (Weihs 1980, Pinder and Feder 1990). One hypothesis for how such mixing might occur is the through movement of the pectoral fins (e.g. Liem 1981). In experimental studies on larval zebrafish, we found that the pectoral fin activity increased under low-oxygen conditions (Green *et al* 2011). In addition, we observed that the pectoral fin movement transported dye-labeled fluid from locations rostrolateral to the body caudally and toward the body surface. The fins appeared to stretch and fold the fluid as it was transported posteriorly along the trunk, suggestive of mixing. These observations have led us to hypothesize that the pectoral fin movement functions to transport and mix fluid near the body surface.

The kinematics of a limb moving in a fluid can have a strong influence over the resulting flow pattern. We have found that the pectoral fin movement of larval zebrafish is asymmetric, with significant bending occurring along its proximodistal axis during abduction as the fin is moved forward and away from the body, but considerably less during adduction as the fin returns to the body (see figure 1(*A*)). This asymmetric bending is surprising given that the muscle and skeletal morphology of the fin appears symmetric: the two opposing abductor and adductor muscles have equal sizes and thicknesses (Thorsen and Hale 2005), and the plate-like endoskeletal disk that runs between these muscles (Grandel and Schulte-Merker 1998) has no obvious geometric asymmetries. Here we describe the kinematics of fin bending during rhythmic slow swimming. We hypothesize that fin kinematics that includes bending during abduction will result in enhanced fluid mixing in comparison to purely rigid fin kinematics without bending.

We test the hypotheses for the role of the larval pectoral fin in fluid mixing near the body surface using computational fluid dynamics methods developed to study fish locomotion (Curet *et al* 2010; see supplementary videos 1 and 2, available from stacks.iop.org/BB/8/016002/mmedia) in conjunction with a Lagrangian flow analysis (Shadden *et al* 2005, Peng *et al* 2007, Peng and Dabiri 2009). Lagrangian methods address the motion of fluid particles and volumes over time, and are well suited for analyzing fluid transport and mixing problems. Small systems are as yet difficult to examine quantitatively with experimental approaches such as DPIV. In addition, computational modeling allows us to readily manipulate the morphology of the animal in ways that are as yet impossible experimentally. In particular, we address our hypothesis that fin bending is important to fluid mixing by changing fin kinematics in the model to keep the fin straight throughout the abduction–adduction cycle. By examining the fluid flow around the larval zebrafish fins, we aim both to better understand functional adaptations in a viscous flow regime, particularly in early life history, and to examine how biological systems have evolved to contend with issues of fluid mixing.

2. Materials and methods

2.1. Imaging pectoral fin and body movement

We image swimming bouts of five-day post-fertilization, wild-type larval zebrafish (*Danio rerio*) using a high-speed video camera (Basler Vision Technologies A500, Exton, PA) mounted on a dissection microscope (Leica MZ6, Wetzlar, Germany). Video frames are acquired at a rate of 1000 Hz. A high frame rate and magnifying optics are necessary because of the small size (∼0.039 cm) and high movement frequency (∼28 Hz) of the larval pectoral fins. Fish are imaged in a rectangular glass tank (*x*–*y*–*x* dimensions 3 cm × 6.5 cm × 1.5 cm). The focal plane of the camera is fixed at the center of the tank and at mid water depth to ensure that swimming bouts occur away from the walls and floor of the tank. In the majority of experiments, dorsal-view videos are obtained; however, additional experiments are performed using a right angle prism to capture images from a lateral or frontal view. Data from five individuals are used to analyze pectoral fin bending. Movement of the body in this data set was analyzed previously (Green *et al* 2011). Dorsal- and lateral-view images from three different fish are used to build a three-dimensional (3D) model. The total lengths of the body and pectoral fins among these individuals do not vary substantially (range of body lengths: 0.373–0.410 cm; range of pectoral fin lengths: 0.035–0.042 cm).

2.2. Flow visualization using dye

To image the flow pattern generated by the pectoral fin movement, we place drops of methylene blue dye (0.5% diluted in water) near the head using a dulled syringe needle connected to a pressure transducer (Fluke Corporation, Everett, WA). Low-level pressure (∼1 mm Hg) is used to expel dye from the syringe tip. Unlike the free-swimming experiments detailed in section 2.1, dye imaging is performed when fish are near the bottom of the tank. Under this condition, fish do not move forward during swimming possibly due to surface friction or floor boundary layer effects. Lack of forward movement allows easier placement of dye at a consistent location near the head of the fish.

2.3. Measuring and modeling the shape and kinematics of the fins and body

A combination of automated and manual methods is used to track movement and to build a 3D, kinematic model of a swimming larval zebrafish (see supplementary videos 1 and 2, available from stacks.iop.org/BB/8/016002/mmedia). The body and fins are represented as a collection of material points (7869 in total). We approximate the body shape as a series of elliptical cross-sections, and derive body material points from these elliptical sections. The pectoral fins, medial fin fold and caudal fin are represented as thin sheets of material points (one material point in thickness). Geometric parameters of the model are selected to fit the geometry of fish as measured from experimental video data.

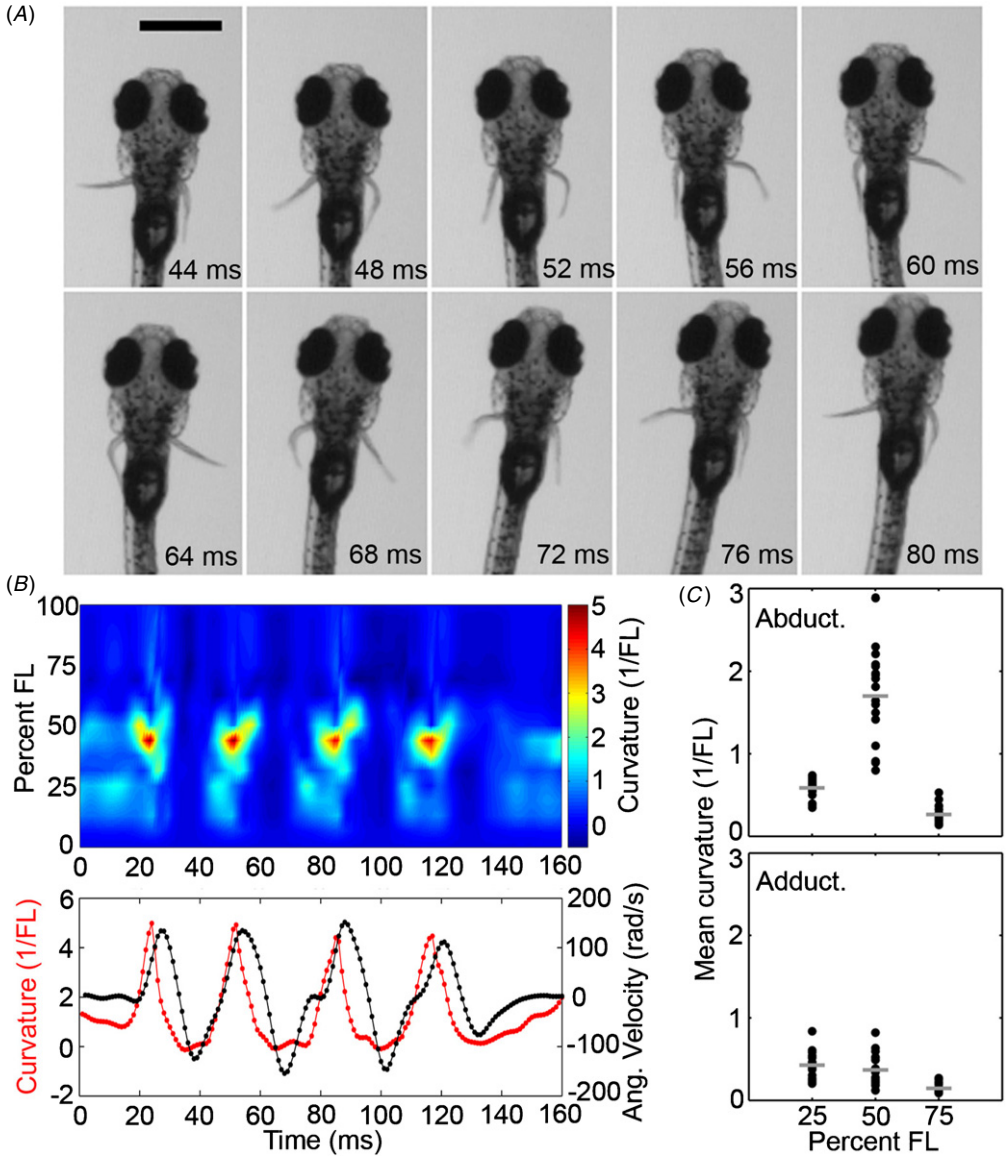

Figure 1. The pectoral fin bends along its proximodistal axis during abduction but remains relatively rigid during adduction. (*A*) Example frames showing an entire (right) pectoral fin beat. Fin abduction occurs from 44 to 60 ms and bending can be seen during this time. Fin adduction is shown from 64 to 80 ms during which the fin appears relatively rigid. Scale bar = 0.05 cm. (*B*) Top panel: the curvature of the right fin shown in (*A*) is plotted at each position along the fin (0–100% fin length (FL)) and at each time during a swim bout. Peaks in the curvature appear red. The location of the peak curvature is consistent across subsequent fin beats, occurring near 44% FL. Bottom panel: curvature at 44% FL (red, left axis) and the angular velocity of the fin tip (black, right axis). Positive angular velocities indicate fin abduction, whereas negative angular velocities indicate fin adduction. (*C*) Mean curvature, averaged over the abduction (top panel) and adduction (bottom panel) periods of the fin beat, is plotted versus position along the length of the fin ($n = 18$ fin beats in five fish). Average values are indicated by gray horizontal bars.

The position of the body midline is tracked in each video frame using a program written in MATLAB (The MathWorks, Natick, MA), which was described previously (Green *et al* 2011). A set of 101 uniformly spaced points on the body midline are used to define the centers of elliptical cross-sections. Ellipse height and width are set equal to manual measurements of body width and height, not including fins and fin fold, from dorsal- and lateral-view video frames. The orientations of the elliptical cross-sections of the body change as the fish swims forward, reflecting the deformation of the body during swimming. Ellipse orientation is determined by computing the normal vector of the body midline at the ellipse center point and orienting the ellipse to be collinear with the normal vector. Roll and pitch rotations of the body during low-speed swimming are small and are not included in the model.

Larval zebrafish have two pectoral fins and a median fin fold that extends along the length of the tail and is continuous with the caudal fin. The shapes of the fin fold and caudal fin are derived from manually digitized points on the margin of the fins in lateral-view video frames. Pectoral fin position and shape are manually measured in dorsal-view video frames by selecting five points along the leading edge, starting at the base of the fin and extending to the distal tip of the fin. A spline

is fitted to these points and a set of 16 new, uniformly spaced points are re-sampled from the spline fit to the leading edge. The shape of pectoral fins in the lateral view is determined from manually digitized outlines. Rigid fins are constructed by constraining the proximodistal axis of the fin to retain a rigid (linear) morphology, by making the proximodistal axis a straight line that intersects the 14th point along the fin, which was near the fin tip (see supplementary videos 3 and 4, available from stacks.iop.org/BB/8/016002/mmedia).

We measure fin bending by computing the curvature (κ) of the leading edge of the pectoral fin, using a standard formula (as in previous work (Green *et al* 2011)):

$$\kappa = \frac{|x'y'' - y'x''|}{[(x')^2 + (y')^2]^{3/2}}, \tag{1}$$

where x and y denote the spatial coordinates of material points on the leading edge of the fin and derivatives are with respect to the leading edge arc length, and are central difference approximations.

2.4. Computational fluid dynamics

We perform computational fluid dynamics simulations using a variation of the fully implicit iterative self-propulsion algorithm (developed in Curet *et al* (2010)) to solve the flow surrounding the zebrafish. The key idea for this method is to assume that the entire fluid–body domain is a fluid. Then, we impose the constraint that the deformation rate tensor associated with the rigid motion component of the swimming body is equal to zero (in other words, the deformation component of the movement of the body and fins is subtracted, and the remaining velocity of movement is constrained to be like a rigid body). A coupled solution in the fluid–body domains gives the swimming velocity of the body and the velocity field of the fluid. For the simulations in this work, we do not solve for the swimming velocity but keep the swimming velocity from the measured kinematics. The simulation domain size is 0.3 cm $\times$ 0.8 cm $\times$ 0.2 cm (x–y–z) with a grid resolution of (N_x, N_y, N_z) = (120, 200, 60). The fluid velocity at the walls is set equal to zero. The density and viscosity of the water were $\rho = 1.0$ g cm^3 and $\mu = 0.01$ g (cm s)$^{-1}$, respectively. The density of the zebrafish is approximated to be equal to water. The time step is equal to 0.0005 s. A detailed convergence test of the computational method was presented in a previous study (Curet *et al* 2010).

2.5. Analysis of flow structures near the pectoral fin

Lagrangian coherent structures (LCS) are fluid surfaces that act as transport barriers and can be used to identify dynamically distinct fluid regions. LCS are attracting or repelling, so that trajectories of fluid particles either converge toward the LCS or expand away from the LCS. For two-dimensional (2D) flows, LCS are identified as ridges in the finite-time Lyapunov exponent (FTLE) field (Shadden *et al* 2005). To compute FTLE fields, we use the velocity fields from our simulations and code written in MATLAB and maintained by the Biological Propulsion Laboratory at the California Institute of Technology (LCS MATLAB Toolkit, http://dabiri.caltech.edu/software.html) (see Peng *et al* (2007) and Peng and Dabiri (2009) for additional examples of this method). Fluid velocities have three spatial dimensions, and are defined at points on a 3D grid; however, we simplify our analysis of flow structures by using only those velocity vectors defined at points in a 2D, horizontal plane that intersects the pectoral fins midway through their dorsoventral depth, and the components of these velocity vectors within this plane (ignoring the vertical components). This 2D analysis of a 3D flow is validated to capture the major structural features of the flow around the pectoral fins in section 3.2.

The LCS and the FTLE are rigorously developed in Shadden *et al* (2005). We briefly repeat the essential definitions here. The position of a fluid particle through time as it is advected by the flow is given by the flow map ϕ. Specifically, if the fluid particle is initially located at position X_0 at time T_0, then after a time interval of length T, the position X of the particle is given by

$$X = \phi_{T_0}^{T_0+T}(X_0). \tag{2}$$

The FTLE can be obtained by computing the matrix norm of the Jacobean of the flow map. The Jacobean of the flow map is given by

$$J = \frac{\mathrm{d}\phi_{T_0}^{T_0+T}}{\mathrm{d}X}. \tag{3}$$

The matrix norm of the Jacobean is defined as

$$\|J\|_2 = \sqrt{\lambda_{\max}(J * J)}, \tag{4}$$

where $\lambda_{\max}(J^*J)$ is the maximum eigenvalue of the matrix J^*J (the adjoint of the matrix J is denoted as J^*). The FTLE is defined as

$$\sigma_{T_0}^{T_0+T}(X) = \frac{1}{T}\log(\sqrt{\lambda_{\max}(J * J)}). \tag{5}$$

For a more intuitive viewpoint, consider two fluid particles separated by a small displacement vector $\delta(0)$. Suppose the displacement vector between the particles after a time T is $\delta(T)$. If the initial displacement vector $\delta(0)$ is chosen along the direction of the eigenvector associated with the maximum eigenvalue $\lambda_{\max}(J^*J)$, then

$$\|\delta(T)\| = \sqrt{\lambda_{\max}(J * J)}\|\delta(0)\|. \tag{6}$$

This implies that the final distance between two fluid particles is proportional to the initial distance, with a constant of proportionality equal to the matrix norm of the Jacobean of the flow map. If this constant is less than or equal to 1, then the final distance between particles will be less than or equal to the initial distance and particles will remain close together after a time interval T. However, if this constant is greater than 1, then the final distance between particles will be greater than the initial distance and particles will expand away from each other over the time interval T.

Equation (6) can be re-written in terms of the FTLE:

$$\|\delta(T)\| = e^{T\sigma_{T_0}^{T_0+T}(X)}\|\delta(0)\|. \tag{7}$$

Thus, for positive FTLE values, particles expand away from each other exponentially. For zero or negative FTLE values, particles remain near each other.

To numerically compute the FTLE field, the LCS MATLAB toolkit seeds the fluid domain with fluid particles and uses the numerical integration and the fluid velocity field to compute the trajectories of fluid particles over a specified time interval going either forward (to find repelling LCS) or backward in time (to find attracting LCS). The Jacobean of the flow map is computed using the initial and final positions of fluid particles and central difference derivatives. Finally, the matrix norm of the Jacobean is computed using built-in MATLAB functions.

Simulations and subsequent FTLE calculations are performed using data from a single swimming bout. During this swimming bout, the fish moves forward; however, using simulations, we also consider the case in which the forward movement is prevented by holding the center of mass of the fish in a fixed position. The latter, 'fixed-position' case is used to compare our computational results to flow visualization experiments, in which fish perform swimming movements but do not move forward (see section 2.2).

The simulated swimming bout includes four pectoral fin beats. FTLE fields and fluid particle trajectories are obtained by numerical integration (the Runge–Kutta method) over a time period of 160 ms, which encapsulates the four fin beats. The forward-time FTLE, which is used to visualize repelling coherent structures, is computed by integrating from time 0 ms (slightly before the initiation of fin movement) to time 160 ms (slightly after the fins stop beating). The backward-time FTLE, which is used to visualize attracting coherent structures, is computed by integrating from time 160 ms to time 0 ms.

2.6. Calculation of Reynolds number and Peclét number

We compute the Reynolds number (*Re*) associated with the pectoral fin movement, using the formula

$$Re = \frac{UL}{\nu}, \tag{8}$$

where U is set equal to the mean or maximum linear speed of the distal tip of the pectoral fin, the characteristic length L was set equal to the proximodistal fin length (FL) and $\nu = 0.95 \times 10^{-6}$ m^2 s^{-1} is the kinematic viscosity of water near room temperature. The Reynolds number indicates the relative importance of inertial and viscous forces involved in the movement of an object through a fluid, with $Re < 1$ indicating viscosity-dominated flows, and $1 < Re < 100$ indicating an intermediate flow regime in which viscous and inertial forces are significant.

We also compute the Peclét number (Pe), which measures the relative importance of advection and diffusion in the transport of mass, such as dissolved oxygen within a fluid. Pe was calculated using the formula

$$\mathrm{Pe} = \frac{UL}{D}, \tag{9}$$

where $D = 1.97 \times 10^{-5}$ m^2 s^{-1} is the diffusion coefficient of dissolved oxygen in water near room temperature. For Peclét number calculations, we again use a characteristic length $L =$ FL (fin length) and set U equal to the mean or maximum linear speed of the fin tip.

3. Results and discussion

3.1. Pectoral fin bending, Reynolds number and Peclét number

A bending asymmetry along the length of pectoral fin is consistently evident during fin beats, with the fin bending back during abduction and remaining relatively straight during adduction (figure 1(*A*)). Measurement of fin bending from 18 fin beats in five fish demonstrates high levels of curvature, with an average maximum of 4.44 $\pm$ 1.07 FL^{-1} (mean $\pm$ s.d.) at an average of 47 $\pm$ 4% (mean $\pm$ s.d.) of the fin length (FL) along its proximal to distal axis during abduction. During the fin beat cycle, bending develops at the beginning of abduction and persists until adduction is initiated. The times of maximum fin curvature occur near the times of maximum fin angular velocity during abduction (figure 1(*B*)). During fin adduction (signified by periods of negative angular velocity in figure 1(*B*)), the curvature of the fin is near zero with an average maximum curvature of 1.55 $\pm$ 0.54 FL^{-1} (mean $\pm$ s.d.) at 37 $\pm$ 10% (mean $\pm$ s.d.) along the fin.

Comparing average curvature at 25% increments along the fin (25%, 50% and 75% FL) demonstrates that the curvature at 50% FL is significantly greater than more proximal or distal positions, which indicates that this curvature is localized to mid-fin (figure 1(*C*), $P < 10^{-7}$ for comparison between 25% and 50% FL and $P < 10^{-8}$ for comparison between 50% and 75% FL, *t*-test with Welch's correction for unequal variances). Average curvature at 25% and 50% FL is not significantly different during adduction ($P = 0.33$); however, average curvature at 50% FL is slightly, but significantly larger than average curvature at 75% FL ($P < 10^{-3}$) indicating that bending during adduction is localized to the proximal half of the pectoral fin. At all tested locations along the fin, the curvature during adduction is significantly lower than during abduction (figure 1(*C*)). This effect is the largest at 50% FL, where the mean curvature is 0.37 $\pm$ 0.19 FL^{-1} during adduction versus 1.70 $\pm$ 0.55 FL^{-1} during abduction, $P < 10^{-8}$.

The variation in movement between abduction and adduction raises the question of how such differences in a movement pattern are generated. The asymmetry in fin bending occurs despite grossly similar overall muscle morphology and motoneuron physiology between the abductor and the adductor. The anatomy of the larval zebrafish pectoral fin, described previously in Grandel and Schulte-Merker (1998) and Thorsen and Hale (2005), has shown that the basic structure of the fin in the larval zebrafish includes an endoskeletal disk with fan-shaped sheets of muscle, the abductor and the adductor, on either side. While details of muscle fiber recruitment are not known, at this stage of development, there is no obvious muscle subdivision into discrete fascicles. Physiology of both fin nerves and individual motor neurons during fictive slow swimming shows similar durations and levels of activity between adductor and abductor motor pools and no overlap in activity between the periods that the abductor and adductor are active. Peripheral to the muscular region of the fin, a fin membrane extends for 192% of the length of the muscle. The location of peak bending is

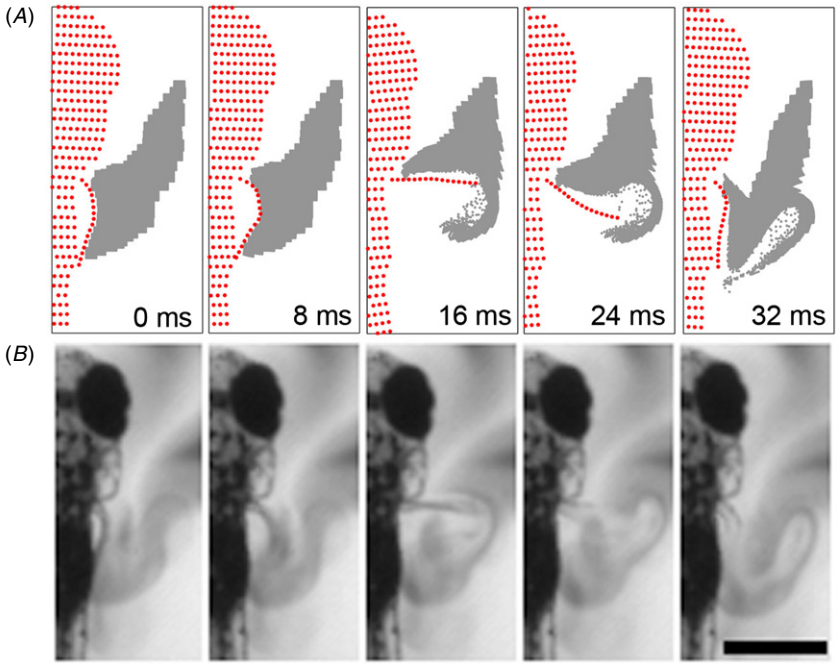

Figure 2. Simulations capture geometric features of fluid motion near the fin. (*A*) Five successive frames showing a single fin beat in a simulation. Red dots are material points and the time stamps in the lower right time elapsed from the first frame at the top left. Simulation frames were chosen to match the phases of the fin beat shown in experimental frames directly below. The gray region of fluid is composed of densely spaced fluid particles. (*B*) Five successive frames showing a single fin beat in a dye-imaging experiment. The geometry of fluid stretching and folding is comparable between each frame of the simulation (*B*) and the experiment (*A*). Near the peak of pectoral fin abduction (16 ms), a fold is formed in the simulated particles and in the dye-marked fluid, which is then stretched back toward to form a loop-shaped fluid fold (32 ms). The shape and position of the fold structure is consistent between the simulation and the experiment. Scale bar = 0.05 cm.

near the membranous region at the border with the muscle bundle. The mechanical properties of the fin membrane are not known.

That asymmetry in fin bending occurs even when there is no forward movement of the fish, which would add to the drag force experienced by the fins during abduction, suggests that the difference in fin bending during abduction and adduction is not merely an unavoidable effect of body-induced flow during swimming. We suggest that asymmetry in the material properties of the fin, an interaction effect with the body surface or subtle active control of fin muscles allows for these different movement patterns in the abduction and adduction phases of the fin cycle. Greater examination of other fin behaviors, modeling of the forces on the fin and analysis of the fins' mechanical properties will be important for further understanding of the larval pectoral fin as a functional system.

The Reynolds number (*Re*) associated with the pectoral fin movement, measured for the fin movement in five fish (with an average fin length (FL) of 0.039 $\pm$ 0.003 cm), is $Re = 25 \pm 6$ when the fin tip had a maximum linear speed of $6.10 \pm 1.10\,\mathrm{cm\,s^{-1}}$, and $Re = 10 \pm 6$ using the average fin tip speed ($2.35 \pm 0.69\ \mathrm{cm\ s^{-1}}$). These Reynolds number values indicate that the pectoral fins move in a flow regime in which viscous forces are very significant but do not dominate over inertial forces. Moreover, little or no turbulence is expected to occur in the flow around the pectoral fins. The Peclét number was $\mathrm{Pe} = 1210 \pm 280$ at maximum fin tip speed, and $\mathrm{Pe} = 467 \pm 157$ using the average fin tip speed. These Pe values are much greater than 1, indicating that at the length scale and speed of fluid flow around the pectoral fin, advection dominates over diffusion in the transport of dissolved oxygen. In previous work, we demonstrated that forward swimming without the pectoral fin movement results in the separation of upstream fluid from the body surface, with an intervening boundary layer of fluid enveloping the body (Green *et al* 2011). Larval zebrafish respire by absorbing dissolved oxygen through the skin, so fluid in the boundary layer region around the body surface, which has a lateral thickness comparable both to the body width and to the length of the pectoral fin, may become depleted in oxygen over time (Weihs 1980). At a high Peclét number, advection of fluid is required to rapidly increase dissolved oxygen concentration in the region surrounding the body by bringing distant fluid toward the body and mixing it with fluid near the body surface.

3.2. Comparison of experimental and simulated flow patterns

To demonstrate the validity of our Lagrangian analysis of flow structures near the pectoral fin, we compare simulated flow patterns to experimentally measured flow patterns near the pectoral fin. As detailed in section 2.5, we used the 'fixed-position' case, in which the position of the center of mass of the model fish was held fixed, to compare simulations to flow visualization experiments. We populated a fluid region near the fin with densely spaced tracer particles to mimic the placement of dye in experiments (figure 2(*A*)). A visual comparison of successive stages of the fin beat demonstrated a close match between the experimental and simulated flow

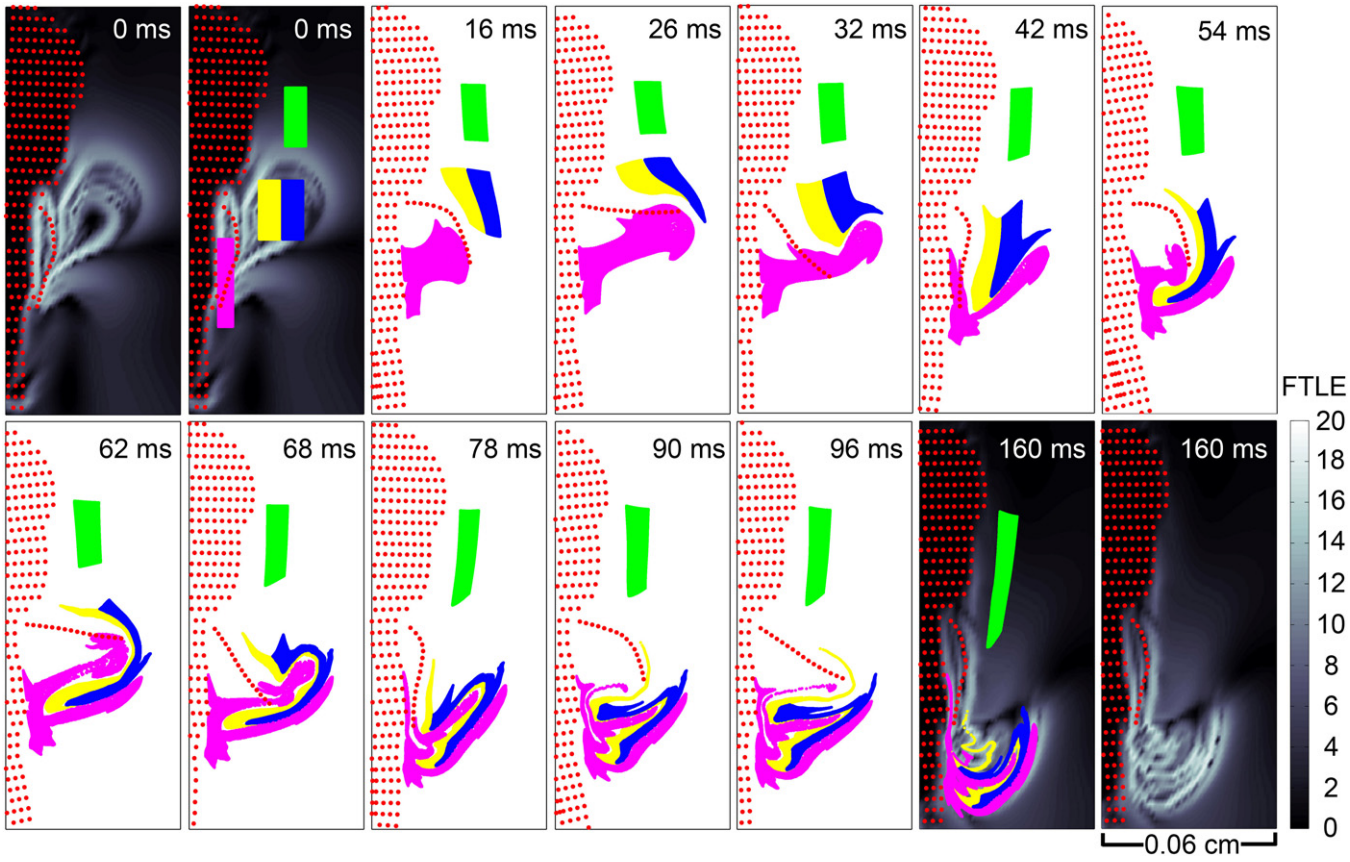

Figure 3. Pectoral fin beats mix fluid near the side of the body with fluid anterior and lateral to the fins. In this simulation, the position of the center of mass of the fish was held in a fixed position. A series of frames showing fluid motion, starting from the upper left, and spanning four fin beats are shown (time elapsed from the first frame is marked at the upper right corner of each frame). Three regions of densely spaced fluid particles were given different colors to illustrate mixing (yellow, blue and magenta). The top left frame (0 ms) shows the forward-time FTLE field. Yellow and blue particles were launched from inside the region enclosed by the outer ridge (repelling LCS, second frame, 0 ms), whereas green particles were initially placed outside this region. Magenta particles were placed near the side of the body. During abduction (16, 54 and 90 ms), magenta fluid is stretched away from the body. During adduction (32 and 68 ms), yellow and blue fluid is stretched toward the body and transported posteriorly. Folds in the yellow and blue fluid are formed during each fin beat as the fin reverses its movement direction at transitions between abduction and adduction. Stretches of magenta fluid are located between the folds. The bottom right frame (160 ms) shows the backward-time FTLE field, in which a closely layered series of ridges is visible, indicating the location of attracting LCS. The final positions of fluid particles are distributed along the attracting LCS. The scale bar for FTLE plots is shown at the bottom right, with FTLE values less than or equal to zero plotted in black.

patterns (figures 2(*A*) and (*B*)). In both the experimental and simulated cases, the fin beat appeared to stretch and fold dye-marked fluid into a loop-shaped pattern, and the position of this loop, relative to the position of the fin, was consistent in the simulation and the experiment.

3.3. Flow structures and fluid transport during normal pectoral fin beats

We next examine fluid transport and flow structures near the pectoral fin during normal fin beats under two movement conditions: (i) the fixed-position case and (ii) the case in which the fish is allowed to swim forward normally, matching the original, experimentally measured kinematics.

Flow structures and transport of fluid regions for the fixed-position case are illustrated in figure 3. Ridges in the forward-time FTLE field, located anterior and lateral to the pectoral fin, indicate the presence of repelling LCS anterior and lateral to the fin (figure 3, time $T = 0$ ms). Repelling LCS form nearly closed loops. Fluid inside the region bounded by the outer, repelling LCS (yellow and blue fluid regions in figure 3) is captured by fin beats, transported backward and mixed with fluid near the side of the body (magenta fluid region in figure 3), whereas fluid outside this region was not mixed by fin beats (green fluid region in figure 3). Fluid captured by fin beats is stretched and folded, resulting in a series of closely spaced fluid layers in the fin wake after four fin beats (figure 3, $T = 160$ ms). These fluid layers line up along tightly spaced, attracting LCS in the backward-time FTLE field. Fluid particles initially located near the body surface (figure 3, magenta particles) are transported outward from the body in a lateral direction, and these particles fill the regions between the layers of fluid that are transported backward by fin beats.

The flow pattern in the fixed-position case indicates that pectoral fin beats capture fluid from a region located anterior and lateral to the fin, and transport this fluid backward while simultaneously stretching and folding the transported fluid. At the same time, fin beats transport fluid near the body

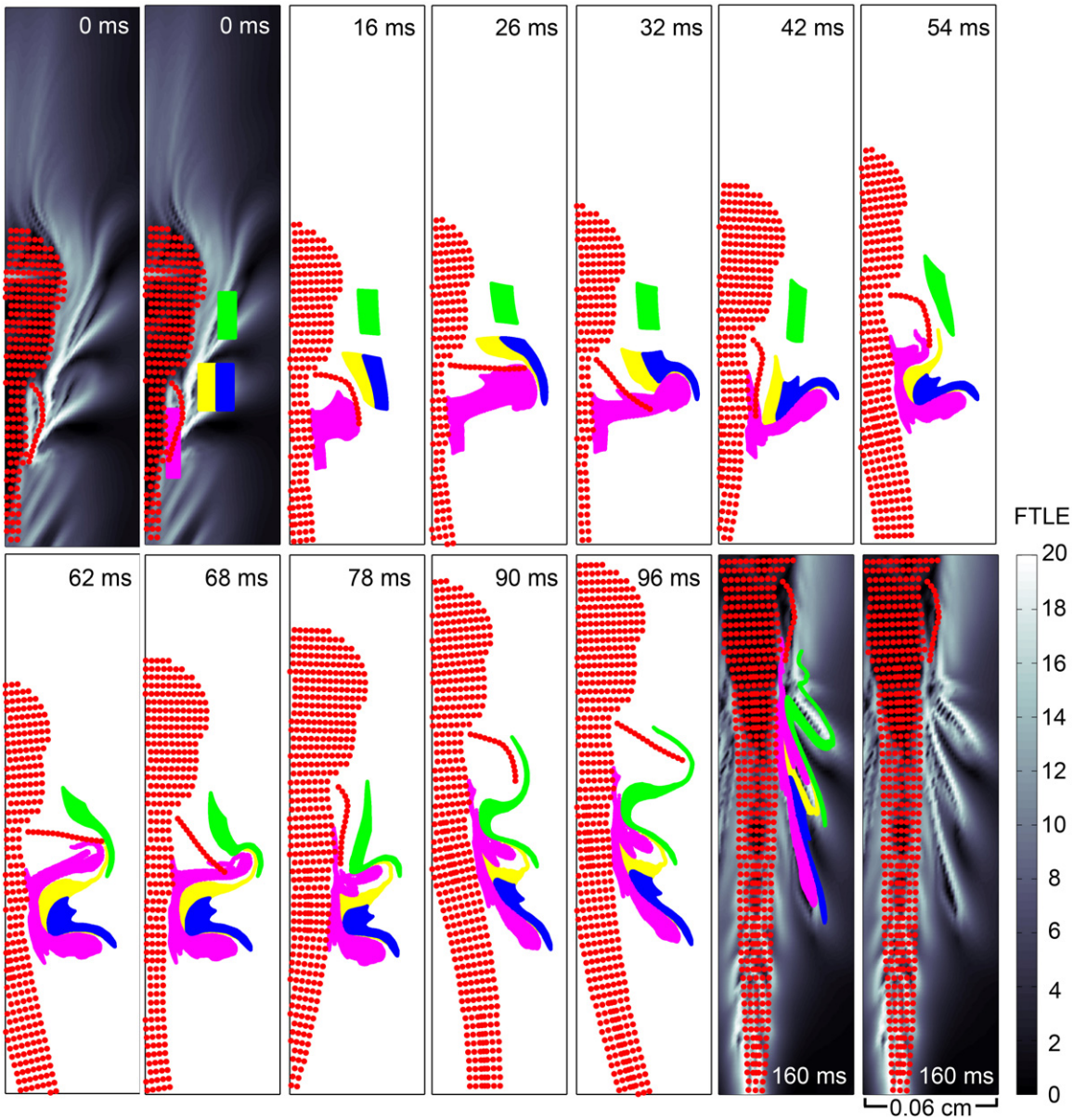

Figure 4. During forward swimming, pectoral fin beats mix fluid near the side of the body with fluid anterior and lateral to the fins; however, in this case, transported fluid is not as tightly layered as in the case when there is no forward movement of the body (see figure 3). A series of frames, starting from the upper left, and spanning four fin beats are shown (time elapsed from the first frame is marked at the upper right corner of each frame). Four regions of densely packed fluid particles were tagged with colors to illustrate mixing (yellow, blue, green and magenta), and launched from the same initial positions as in figure 3. The top left frame shows the forward-time FTLE field, in which a series of ridges extend from the pectoral fin, indicating the location of repelling LCS upstream of the fin. As in figure 3, magenta fluid is stretched away from the body during abduction (16, 54 and 90 ms). During adduction, yellow, blue and green fluid is stretched toward the body (32 and 68 ms). The bottom right frame shows the backward-time FTLE field, in which a series of ridges is visible, indicating the location of attracting LCS. The final positions of tagged fluid particles are distributed along the attracting LCS. The scale bar for FTLE plots is shown at the bottom right, with FTLE values less than or equal to zero plotted in black.

surface laterally to fill the regions between folds of stretched fluid that was originally located upstream. This effect creates closely spaced interfaces between the fluid regions, which would be predicted to decrease the time needed for mixing of substances, such as dissolved oxygen, between fluid regions by diffusion. The rhythmic beats of respiratory cilia in the lungs of vertebrates such as humans also display asymmetric bending and computational simulations have shown that ciliary beating creates striated flow patterns and strong LCS in nearby fluid (Lukens *et al* 2010). Striated flow patterns have been found to lead to effective mixing at lower Reynolds numbers and higher Peclét numbers in engineered devices such as microfluidic channels (e.g. Strook *et al* 2002, Ottino and Wiggins 2004).

We next examined the fluid flow around the pectoral fin during the forward swimming case (figure 4). The forward-time FTLE field shows repelling LCS extending outward from the pectoral fin in the anterior and lateral directions, and sequentially arranged along the direction of swimming (figure 4, $T = 0$ ms). Repelling LCS do not form strong loops as seen in the fixed-position case, so the regions of

fluid captured by fin beats are not as obviously demarcated; however, fluid particles initially placed at positions between the repelling LCS (green, yellow and blue particles in figure 4) are transported backward, stretched and folded by fin beats. Layers of transported fluid align along attracting LCS shown in the backward-time FTLE field (figure 4, $T = 160$ ms). Fluid initially located near the body surface (magenta, figure 4) is transported laterally to fill the regions between layers of the stretched and folded fluid that was initially located upstream.

Our results suggest that the flow pattern near the pectoral fins is significantly altered when the fish does not move forward. In the fixed-position case, the fins capture fluid from a single region, located anterior and lateral to the fin, that is strongly demarcated by repelling LCS. Due to the lack of forward translation, each fin beat samples fluid from the same capture region. In contrast, during the forward swimming case, the fin captures fluid from multiple regions as the fish translates forward. Fluid in each region is sampled by a single pectoral fin beat instead of multiple fin beats, and this could explain why the repelling LCS in the forward swimming case lack the same strongly demarcated distal boundaries as shown in the fixed-position case. Differences in the flow pattern between the fixed-position and forward swimming cases are also seen at the end of the bout and in the shape of the attracting LCS. In the fixed-position case, fluid layers and attracting LCS in the fin wake are oriented more laterally and the distance between fluid layers is smaller. In the forward swimming case, fluid layers in the fin wake are sheared along the direction of forward translation, which changes the orientation of attracting LCS to be more aligned with the direction of travel. The distance between fluid layers in the fin wake appears somewhat larger in the forward swimming case, suggesting that mixing by the pectoral fin may not be as effective during the forward movement.

Previously, we observed an increase in the frequency of bouts of fin movement without any accompanying movement of the tail (fin-only bouts) when fish were placed in an oxygen-deprived environment (Green *et al* 2011). During fin-only bouts, the forward movement of the body is greatly diminished due to the lack of tail movement. The results of our simulations suggest that bouts of rhythmic pectoral fin movement, without any corresponding forward movement of the body, can mix upstream fluid with fluid near the body surface. Mixing via stretching and folding of fluid by the fins still occurs during the forward movement, but mixing appears less pronounced under this condition, due the larger distances between fluid layers. Differences in the strength and size of LCS near a swimming animal when the position of the animal is held fixed versus when the animal is allowed to translate forward have also been demonstrated in computational studies of jellyfish swimming at low/intermediate Reynolds numbers (Wilson *et al* 2009). Pectoral fin-only movement bouts may be an energetically efficient way to mix fluid near the body, since these movements do not involve the recruitment of the much larger axial muscle mass. Future experimental or computational work may be able to test this hypothesis.

3.4. Flow structures and fluid transport during rigid fin beats

To test the role of fin bending in fluid transport, we examine the fluid flow near the fin when the shape of the fin remains rigid throughout the fin beat. In order to compare the flow around the rigid fin to the flow around the normal fin, we compute FTLE fields over the same integration time windows, and launch color-tagged fluid particles from the same initial positions as in the normal fin movement case detailed in section 3.3. We simulate two cases: (i) the fixed-position case and (ii) the forward swimming case; however, we obtain similar results for the comparison between rigid and normal fins in both these cases and we only describe the fixed-position case for brevity.

A comparison of the LCS geometries and flow patterns generated by rigid and normal fin beats is shown in figure 5. In comparison to normal fin beats, rigid fin beats are less effective in transporting fluid backward, in a posterior direction along the body. This difference is the strongest for fluid that is initially near the body surface (magenta particles, figure 5), but is also visible in the movement of fluid that was distant from the body surface (green, blue and yellow particles, figure 5). The maximum displacement of fluid near the body surface (magenta) in the posterior direction is 0.026 cm after four rigid fin beats versus 0.046 cm after four normal fin beats. This corresponds to a 77% increase in the posterior movement of fluid near the body surface during normal fin beats versus during rigid fin beats. The maximum displacement of fluid distant from the body surface (green, blue and yellow) in the posterior direction is 0.054 cm after four rigid fin beats versus 0.061 cm after four normal fin beats. This corresponds to a 13% increase in the posterior movement of fluid distant from the body surface during normal fin beats versus during rigid fin beats. The increase in posterior transport of fluid near the body surface during the normal fin movement could also be observed from the shape of attracting LCS in the fin wake. Near the body surface, attracting LCS did not extend as far in the posterior direction in the rigid fin movement case as compared to the normal fin movement case (figure 5). The maximum lateral displacement of fluid regions and the lateral span of attracting LCS are nearly identical between normal and rigid fin movement cases.

These results indicate that fin bending increases posterior transport of fluid near the body surface while minimally affecting lateral stretching and folding of fluid. Previous work (Liem 1981) on pectoral fin-generated flows in the larvae of *Monopterus albus* (an eel-like air-breathing fish native to southeast Asia) suggests that the posterior direction of fin-generated flows near the body surface can enhance cutaneous respiration by traveling opposite to the direction of blood flow, which runs anteriorly in the region just below the skin and near the fins. Near the body surface of larval zebrafish, fluid motion in a posterior direction during swimming is decreased by a boundary layer effect (Müller *et al* 2008). Our results provide support for the hypothesis that a counter-current mechanism for respiration is also implemented by pectoral fin beats in larval zebrafish, and that fin bending may be important to enabling this mechanism by increasing transport of fluid near the body surface in a posterior direction. An additional hypothesis is that fin bending may increase the

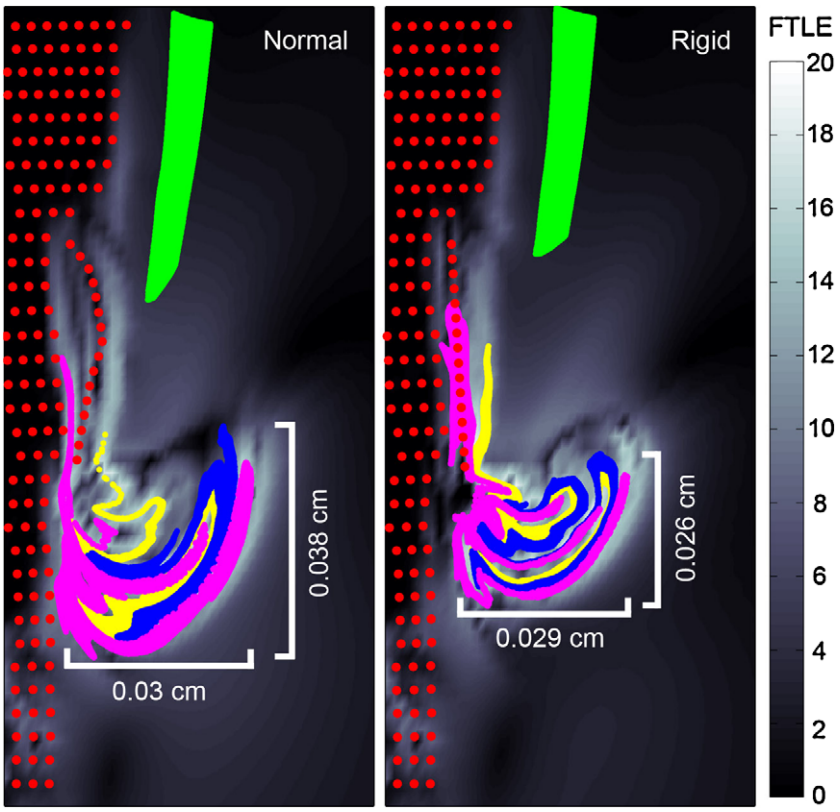

Figure 5. Comparison of flow patterns following rigid and normal fin movement. Left frame: the final position of color-tagged fluid regions after four normal pectoral fin beats is plotted on top of the backward-time FTLE field. The initial positions of these fluid regions are the same as shown in figures 3 and 4. Scale bars indicate the size of the fluid structures in the fin wake along the anterior–posterior axis (vertical) and the proximal–lateral axis (horizontal). Right frame: the final position of color-tagged fluid regions (same initial positions as in the left frame) after four rigid pectoral fin beats is plotted on top of the backward-time FTLE field. After rigid fin beats, the fluid structures in the fin wake do not extend as far in a posterior direction as in normal fin beats (this is seen by comparing the vertical positions of horizontal scale bars placed at the base of the flow structures), but flow structures have nearly identical lateral widths.

efficiency of fin beats by reducing the hydrodynamic force on the pectoral fin during abduction. Future examination of fluid forces on the pectoral fin will be able to further test these hypotheses.

4. Conclusion

Mixing at low/intermediate Reynolds numbers is dependent on stretching and folding of fluid (Ottino 1989). Stretching and folding expand the interfaces between fluid regions and decrease the distance between fluid layers, leading to faster mixing by diffusion. Here we show that the pectoral fins of larval zebrafish effectively mix fluid near the surface of the body in a low Reynolds number, high Peclét number fluid environment, where the mixing processes are dominated by advection (i.e. stretching and folding of fluid) rather than diffusion. This work supports previous experimental studies (Green *et al* 2011) that suggested the function of rhythmic fin movements in respiration by demonstrating that the fins move distant fluid toward the body surface, exchanging and mixing it with fluid in the boundary layer, which could aid respiration by increasing the concentration of dissolved oxygen near the body surface.

We found that bending of the fin during the abduction phase of the fin stroke increases the posterior transport of fluid near the body surface, but does not greatly affect fluid stretching and folding lateral to the body, contrary to our hypothesis that fin bending was critical for effective mixing. This increase in the posterior movement of fluid near the body surface during fin bending may enable more efficient exchange of dissolved oxygen at the skin, as has been demonstrated in other species (Liem 1981). It is also possible that fin bending reduces the energy expended in beating the fins. Further examination of the development of fin movement and respiratory function though larval and juvenile stages using experimental and computational approaches will be necessary to understand the coordination of the fins multiple functions with growth and other ontogenetic changes.

Acknowledgments

We thank Michael LaBarbera for help with aquarium construction and Ru Yi Teow for help with fish care. We thank Drs Joseph Fetcho, Jason MacLean and Nicho Hatsopoulos and members of the Hale lab for feedback on the work. This work was supported by NSF (IBN043977) and ONR (N000140910352) grants to MEH.

References

Curet O M, AlAli I K, MacIver M A and Patankar N A 2010 A versatile implicit iterative approach for fully resolved simulation of self-propulsion *Comput. Methods Appl. Mech. Eng.* **199** 2417–24

Grandel H and Shulte-Merker S 1998 The development of paired fins in the zebrafish (*Danio rerio*) *Mech. Dev.* **79** 99–120

Green M H, Ho R K and Hale M E 2011 Movement and function of the pectoral fins of the larval zebrafish (*Danio rerio*) *J. Exp. Biol.* **214** 3111–23

Hale M E 1996 The development of fast-start performance in fishes: escape kinematics of the Chinook Salmon (*Oncorhynchus tshawytscha*) *Am. Zool.* **36** 695–709

Hunter J R 1972 Swimming and feeding behavior of larval anchovy *Engraulis mordax Fish. Bull., USA* **70** 821–38

Liem K L 1981 Larvae of air-breathing fishes as countercurrent flow devices in hypoxic environments *Science* **211** 1177–9

Lukens S, Yang X and Fauci L 2010 Using Lagrangian coherent structures to analyze fluid mixing by cilia *Chaos* **19** 1–8

McHenry M and Lauder G 2006 Ontogeny of form and function: locomotor morphology and drag in zebrafish (*Danio rerio*) *J. Morphol.* **267** 1099–109

Müller U K, van den Boogart J G M and van Leeuwen J L 2008 Flow patterns of larval fish: undulatory swimming in the intermediate flow regime *J. Exp. Biol.* **211** 196–205

Müller U K and Videler J J 1996 Inertia as a 'safe harbor': do fish larvae increase length growth to escape viscous drag? *Rev. Fish Biol. Fish.* **6** 353–60

Ottino J M 1989 *The Kinematics of Mixing: Stretching, Chaos, and Transport* (Cambridge: Cambridge University Press)

Ottino J M and Wiggins S 2004 Introduction: mixing in microfluidics *Phil. Trans. R. Soc.* A **362** 923–35

Peng J and Dabiri J O 2009 Transport of inertial particles by Lagrangian coherent structures: application to predator–prey interactions in jellyfish feeding *J. Fluid Mech.* **623** 75–84

Peng J, Dabiri J O, Madden P G and Lauder G V 2007 Non-invasive measurement of instantaneous forces during aquatic locomotion: a case study of the bluegill sunfish pectoral fin *J. Exp. Biol.* **210** 685–98

Pinder A W and Feder M E 1990 Effect of boundary layers on cutaneous gas exchange *J. Exp. Biol.* **154** 67–80

Shadden S C, Lekein F and Marsden J E 2005 Definition and properties of Lagrangian coherent structures from finite-time Lyapunov exponents in two-dimensional aperiodic flows *Physica* D **212** 271–304

Strook A D, Dertinger A A, Mezic I, Stone H A and Whitesides G M 2002 Chaotic mixer for microchannels *Science* **295** 647–51

Thorsen D H and Hale M E 2005 Development of zebrafish (*Danio rerio*) pectoral fin musculature *J. Morphol.* **266** 241–55

Vlyman W J 1974 Swimming energetics of the larval anchovy, *Engraulis mordax Fish. Bull., USA* **72** 885–99

Weihs D 1980 Respiration and depth control as possible reasons for swimming of northern anchovy, *Engraulis mordax*, yolk-sac larvae *Fish. Bull., USA* **78** 109–17

Wilson M, Peng J, Dabiri J O and Eldredge J D 2009 Lagrangian coherent structures in low Reynolds number swimming *J. Phys.: Condens. Matter.* **21** 204105